Helix Conformations in 7TM Membrane Proteins Determined Using Oriented-Sample Solid-State NMR with Multiple Residue-Specific ^{15}N Labeling

Thomas Vosegaard,* Miya Kamihira-Ishijima,† Anthony Watts,† and Niels Chr. Nielsen*
*Center for Insoluble Protein Structures (inSPIN), Interdisciplinary Nanoscience Center (iNANO) and Department of Chemistry, University of Aarhus, Aarhus, Denmark; and †Biomembrane Structure Unit, Biochemistry Department, Oxford University, Oxford, United Kingdom

ABSTRACT Oriented solid-state NMR in combination with multiple-residue-specific ^{15}N labeling and extensive numerical spectral analysis is proposed to determine helix conformations of large membrane proteins in native membranes. The method is demonstrated on uniaxially oriented samples of ^{15}N-methionine, -valine, and -glycine-labeled bacteriorhopsin in native purple membranes. Experimental two-dimensional ^{1}H-^{15}N dipole-dipole coupling versus ^{15}N chemical shift spectra for all samples are analyzed numerically to establish combined constraints on the orientation of the seven transmembrane helices relative to the membrane bilayer normal. Since the method does not depend on specific resonance assignments and proves robust toward nonidealities in the sample alignment, it may be generally feasible for the study of conformational arrangement and function-induced conformation changes of large integral membrane proteins.

INTRODUCTION

Obtaining information about three-dimensional structures, dynamics, and functionally induced conformational changes of membrane proteins at atomic resolution is a major challenge to gaining insights into function. Although this task is well established for globular proteins, as manifested by more than 30,000 structures in the Protein Data Bank (PDB) (1), the number of structures and complete functional descriptions for membrane proteins and other proteins in insoluble environments is still very limited. Labeling difficulties, purification, and size, especially with associated functionally and structurally stabilizing lipids, prevent the ready use of liquid-state NMR for structural resolution. Difficulties in crystallization explain the relatively small number of structures determined using x-ray diffraction (XRD). For proteins where these traditional structure-determination methods fail, any experiment that sheds light on the three-dimensional arrangement of the protein and function-related conformational changes will be of great value for understanding function.

Over the past decade, major efforts have been invested in the development of solid-state NMR spectroscopy as a viable technique for structural studies of membrane proteins (2–5). So far, solid-state NMR studies on large membrane proteins has mainly been focused on high-precision determination of local structural features, such as measurement of specific interatomic distances (5–8), ligand-receptor interactions (9,10), or conformations of small domains of proteins (8). Along with progress in solid-state NMR methodology, a number of atomic-resolution protein structures from solid-state NMR have recently been presented (11–21). These structures are all of smaller proteins with 50–150 amino acids, determined using magic-angle spinning (MAS) NMR for microcrystalline samples of globular proteins or for smaller membrane peptides/proteins using oriented-sample solid-state NMR with the peptides/proteins oriented macroscopically in phospholipid bilayers. Recently, efforts have been invested in solid-state NMR characterization of larger membrane proteins in the 7 transmembrane-helix (7TM) class, including ''powder''- and oriented-sample studies of bacteriorhodopsin (bR) (22–29) and the G-protein coupled receptor CXCR1 (30), as well as MAS NMR of sensory rhodopsin II (31), although no structures have been presented yet.

With the aim of resolving the structures of large membrane proteins, we recently made a numerical analysis of the potential of oriented-sample solid-state NMR for structural analysis of the commercially important class of 7TM membrane proteins, which includes G-protein coupled receptors (GPCRs) (32). Although the analysis indicated a potential for structural studies using multidimensional experiments for uniformly ^{15}N-, and in particular ^{13}C,^{15}N-labeled proteins of this size, it was also clear that a prerequisite for full structural analysis of uniformly labeled samples is that they align at least as well as demonstrated for a number of smaller membrane-bound peptides reconstituted into phospholipid bilayers (13,14,16,17). For many membrane proteins, however, such a high degree of alignment may be very hard to obtain, since imperfect alignment governed by

Submitted June 22, 2007, and accepted for publication August 30, 2007.

Address reprint requests to Thomas Vosegaard or Niels Chr. Nielsen, Center for Insoluble Protein Structures (inSPIN), Interdisciplinary Nanoscience Center (iNANO), and Dept. of Chemistry, University of Aarhus, Langelandsgade 140, DK-8000 Aarhus C, Denmark. Tel.: 45-8942-3866 (T.V.) or 45-8942-3841 (N.Chr.N.); Fax: 45-8619-6199; E-mail: tv@chem.au.dk or ncn@chem.au.dk.

Editor: Antoinette Killian.

0006-3495/08/01/241/10 $2.00

doi: 10.1529/biophysj.107.116004

mosaic spread appears to be an intrinsic property of a number of smaller peptides/proteins (33–36), as well as for larger membrane proteins in native membranes (37). The key problem is that imperfect alignment translates into significant line broadening and thereby inevitably increases the risks for overlap of resonances, which cannot be resolved even using time-costly experiments with many spectral dimensions. One way to alleviate this problem is to reduce the number of resonances by residue-specific labeling, even though such an approach also reduces the structural information that can be extracted from a single sample. Following this strategy, we recently demonstrated that in combination with numerical spectrum analysis it is indeed possible to obtain structural information in form of conformations of the TM helices, in this particular case for [^{15}N]Met-labeled bR in native purple membranes (27).

In this work, we propose for the first time, to our knowledge, the use of multiple residue specific labeling in combination with extensive computer analysis to establish detailed structural information for large membrane proteins in two-dimensional (2D) arrays using oriented solid-state NMR spectroscopy. By acquiring 2D NMR spectra for several different residue-specifically ^{15}N-labeled samples and exploiting advanced numerical data analysis approaches, the number of resonances in each spectrum is kept sufficiently low to allow a reliable interpretation, and by combining the analysis of spectra with different residue labels, a sufficiently large number of structural constraints is retained. This approach, which in this study is demonstrated for bR in native purple membranes, relieves the requirement for extremely well-aligned samples and opens up exciting new possibilities for structure/conformation analysis of the large class of integral membrane proteins in native environments, which typically is not amenable to XRD and liquid-state NMR, nor can it be aligned sufficiently well to permit the traditional use of oriented solid-state NMR.

MATERIALS AND METHODS

[^{15}N]Gly-, [^{15}N]Val-, and [^{15}N]Met-bR samples were prepared as described elsewhere (25). In brief, the bR was grown from media containing glycine (^{15}N, 98%), L-valine (^{15}N, 98%), and L-methionine (^{15}N, 98%), respectively, from Cambridge Isotope Laboratories (Andover, MA). The purified purple membranes were oriented on the surface of 30 thin glass plates (8 × 8 × 0.06–0.08 mm) (Paul Marienfeld, Lauda-Königshofen, Germany) by slowly evaporating 3 mg/ml (115 μM) of purple-membrane suspension in deionized water. Finally, the air-dried glass plates containing a total of ~20 mg (0.77 μmol) of protein, were controlled to a relative humidity of 75%, stacked, and sealed (38).

NMR spectra were recorded on Bruker Avance 400 and Varian Unity-INOVA 400 spectrometers, the first equipped with a Bruker flatcoil probe and the latter with a home-built ^{15}N/^{1}H double-tuned flat-coil probe, both with coil dimensions sufficiently large to accommodate the stack of ~30 glass plates oriented perpendicular to the external magnetic field. Polarization-inversion spin-exchange at the magic angle (PISEMA) (39) experiments were recorded using a ^{1}H 90° pulse length of 4 μs and CP-MOIST (40) for a duration of 1 ms with radio-frequency (rf) field strengths of ~40 kHz on the two channels. The ^{15}N rf field strength was increased to 45–50 kHz during the SEMA block with the ^{1}H field strength a factor of $\sqrt{3/2}$ lower. A ^{1}H decoupling rf field strength of 65 kHz was used during acquisition. The spectra were recorded using the following number of scans/t_1 increments: [^{15}N]Gly-bR, 16,000/24; [^{15}N]Val-bR, 6480/32; and [^{15}N]Met-bR, 8600/32, with repetition delays of 1.5 s. For all experiments, the ^{1}H and ^{15}N transmitters were placed at 10 and 130 ppm, respectively, using ^{15}N ppm reference to liquid ammonia by an external $^{15}NH_4Cl$ powder sample at 39.8 ppm and ^{1}H ppm reference to tetramethylsilane by external water solutions. All NMR spectra were recorded at −20°C to reduce the effect of sample heating and improve cross-polarization efficiency. The low temperatures were achieved using an FTS cooling system (FTS Systems, NY) with an air flow of 20 L/min. The indirect axis of the PISEMA spectra was scaled by a factor of $\sqrt{3/2}$ to compensate for the down-scaling of the ^{1}H-^{15}N dipolar coupling by homonuclear decoupling.

RESULTS AND DISCUSSION

Solid-state NMR on uniaxially oriented samples enables direct correlation between the resonance frequencies of the nuclei residing in the protein backbone and the orientation of the peptide planes to which they belong, relative to the bilayer normal (in the situation investigated here, parallel to the external magnetic field). This feature is seen in two-dimensional PISEMA (39) spectra, which, through correlation of ^{1}H-^{15}N dipole-dipole coupling and ^{15}N chemical shift of the backbone amides, give characteristic wheel-like patterns for the transmembrane helices of uniformly ^{15}N-labeled peptides. The shape and position of the wheel pattern, referred to as a polarization-index slant-angle (PISA) wheel, depends on the helix geometry and its orientation relative to the membrane (32,41,42). The major challenge in the analysis of membrane proteins with more than one transmembrane helix is to resolve all resonances and assign them to individual helix PISA wheels. This task is complicated by the fact that for similarly oriented helices, the wheels may have a very similar appearance, since the wheel shape depends mainly on the helix conformation but only very little on the primary sequence. This implies that even for samples displaying a very high degree of alignment, a PISEMA experiment would be able to resolve ~50% of the ^{15}N resonances for typical 30 kDa membrane proteins (32). For large membrane proteins, this situation may be further complicated by larger disorder of the alignment (37) leading to broader resonances and, thereby, poorer spectral resolution.

In this study, we reduce the resolution problem by simultaneous analysis of multiple samples with different residue-specific ^{15}N labeling. This approach has several advantages: 1), each spectrum will be less crowded due to a reduced number of resonances; 2), the separation of resonances from different amino acids into different spectra creates an appreciable difference between the different helices since they differ in primary sequence, and 3), using several samples with labeling of different amino acids, it is possible to obtain a large number of structural constraints in a combined analysis. In the following, we will demonstrate the power of this approach on bR, which is significantly larger than other proteins so far subjected to detailed structural investigation

by oriented-sample solid-state NMR. In a preliminary study of [^{15}N]Met-bR (27), we demonstrated that even in the case of broad resonances and apparent low resolution, it is possible to exploit the fact that the resonance positions provide, in a sensitive manner, information about the orientation of the peptide plane rather than amino acid assignment, with minor perturbations due to secondary structure as typically encountered in liquid-state or non-oriented-sample solid-state NMR spectra. This orientational dependence of chemical shift implies that any lineshape information (e.g., elongated, curved shape), or uneven intensity distribution present for the broad resonances in 2D PISEMA or ^{1}H, ^{15}N chemical shift correlated spectra, may numerically be deconvoluted to unravel the presence of a given number of resonances with different line positions, lineshapes, and potentially intensity. Although not fully assigned, a reasonable set of resonance positions provides, immediately, a set of accurate constraints on the orientation of the involved peptide planes. This is ascribed to the fact that each pair of ^{15}N chemical shift and ^{1}H-^{15}N dipolar coupling is compatible only with a specific set of orientational angles for the peptide planes, or a certain set of helix-tilt and rotational-pitch angles, provided assumptions on the participation of the peptide planes in helical structures are imposed on the analysis.

To demonstrate this approach, and the power of the numerical analysis of oriented solid-state NMR spectra, a numerical test was carried out based on the known structures of the M1 and M2 helices of the sarcoplasmic reticulum calcium ATPase (43) with ^{15}N labeling of the alanine residues (Fig. 1). As illustrated by the red labels in the ribbon structures (Fig. 1 *a*) and the corresponding helical wheels (Fig. 1 *b*), the M1 and M2 helices contain three and six alanine residues, respectively. To mimic this case as closely as possible with the analysis of the conformation of the helices in bR, the two ATPase helices were replaced with ideal helices with all backbone torsion angles $\phi = -65°$, $\psi = -40°$. For the test, we assume that the two helices are characterized by helix-tilt (τ) and rotational-pitch (ρ) angles $\tau^{M1} = 13.92°$, $\rho^{M1} = 66°$ and $\tau^{M2} = 185.9°$, $\rho^{M2} = 88°$, which, assuming typical ^{15}N chemical shielding, ^{1}H-^{15}N-dipolar-coupling tensor parameters, and line widths of 1 kHz in the indirect (^{1}H-^{15}N dipolar coupling) and 10 ppm in the direct (^{15}N-shift) dimension, lead to the ''experimental'' spectrum in Fig. 1 *c*. The very large line widths were chosen to match the condition of ''nonperfectly'' aligned samples, and match well with our previous observations for bR (27). In the experimental spectrum, the crosses represent the true line positions of the nine resonances, whereas the contours reflect the single, but shaped, resonance observed under assumption of the given line widths. The task is now to extract information about the helix orientations from this spectrum using knowledge from the primary sequence alone, along with assumptions on the torsion angles and typical sizes of the chemical shift and dipolar coupling parameters.

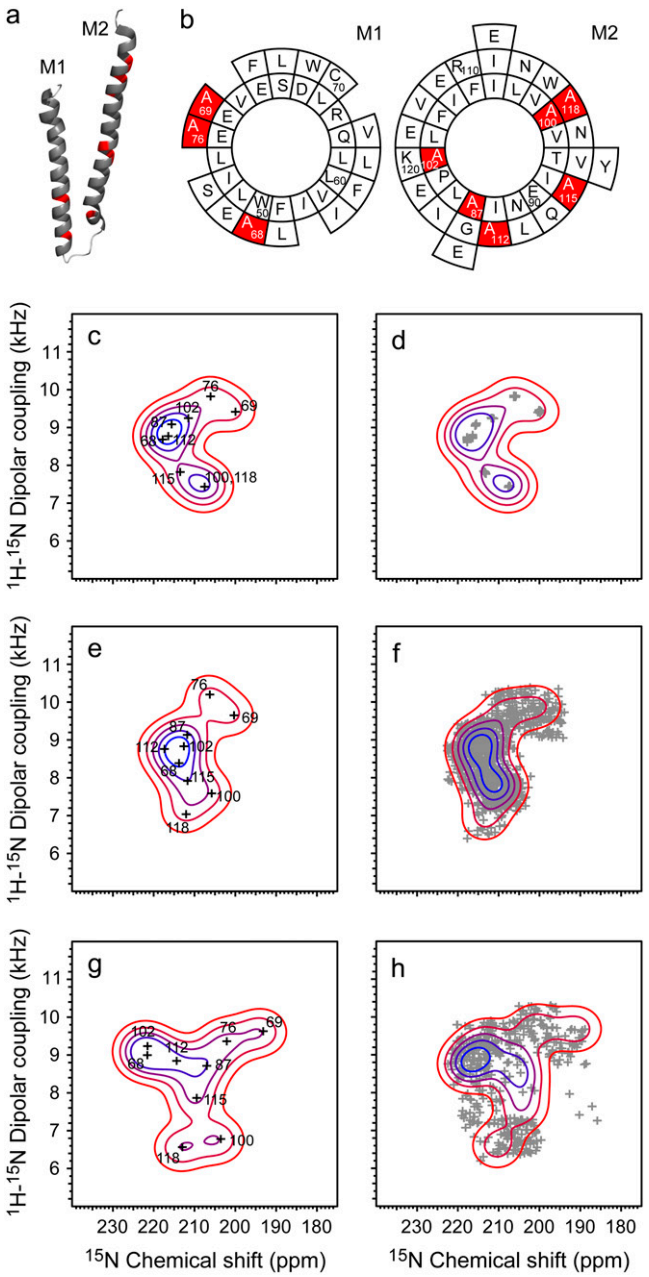

FIGURE 1 (*a*) Structure of the M1 and M2 TM helices of the Ca^{2+} ATPase (43). (*b*) Helical wheel plots of the same helices as in *a*, with the Ala residues highlighted. (*c*, *e*, and *g*) Simulated PISEMA spectra employing ideal helices with helix-tilt (τ) and rotational-pitch (ρ) angles $\tau^{M1} = 13.92°$, $\rho^{M1} = -294°$, and $\tau^{M2} = 185.9°$, $\rho^{M2} = -88°$ corresponding to an [^{15}N]Ala-labeled version of the M1, M2 fragment of the Ca^{2+} ATPase. (*c*) Ideal simulation. (*e* and *g*) The same simulation as in *c*, assuming fluctuations of up to ± 5 ppm/± 500 Hz (*e*), and ± 10 ppm/± 1000 Hz (*g*) for the resonance positions in the ^{15}N chemical shift/^{1}H-^{15}N dipolar coupling dimensions. The crosses in *c*, *e*, and *g* represent the resonance positions, and the contour plots represent the spectra resulting from applying line broadening of 10 ppm/1000 Hz in the ^{15}N chemical shift/^{1}H-^{15}N dipolar coupling dimensions. (*d*, *f*, and *h*) Simulated PISEMA spectra and corresponding resonance positions resulting from the 100 best of 500 independent deconvolutions of the broadened spectra in *c*, *e*, and *g*, respectively.

From the primary sequence and information from hydropathy plots, it is reasonable to assume that there are two helices, and that three alanines are present in one helix and six in the other helix, with the given positions in the primary sequence. Combined with the assumption of ideal helix-torsion angles, the latter information ''links'' the orientational constraints of the nine peptide planes (18 angles in total) to the four angles, τ^{M1}, ρ^{M1}, τ^{M2}, and ρ^{M2}, representing the tilt and rotational-pitch angles for the two helices. The remaining free variables concern the lineshape of the resonances, where we assume Gaussian lines with identical line width for all resonances in the two dimensions (i.e., in total, two parameters, the linewidth in the indirect dimension and the linewidth in the direct dimension, are added as free variables in the optimization). To keep the number of variables low, we additionally assume that all resonances appear in the spectrum with equal intensity, in agreement with our previous numerical investigations (32). Using this setup with six free variables, 100 independent optimizations employing random starting values for all six parameters were processed, giving the line positions of the nine resonances. The result is given in Fig. 1 *c*, where the resonance positions for all 100 independent optimizations are given by crosses: virtually all of them overlap, and the ''smeared'' crosses are at the line positions known from the experimental spectrum. The orientations of the helices were determined to be $\tau^{M1} = 14 \pm 1°$, $\rho^{M1} = 66 \pm 5°$, $\tau^{M2} = 186 \pm 1°$, and $\rho^{M2} = 88 \pm 5°$, as listed in Table 1, which agree favorably with the crystallographically determined values used as input values to the experimental spectrum. Also, the overall lineshape in the spectrum is reproduced very well, demonstrating the validity of the approach for a simple system with two helices and a modest number of labels.

To shift the method more toward ''realistic'' experimental spectra, we have repeated the same investigation but now with the experimental spectrum created from the resonance positions calculated from the ideal helices perturbed by scatter of up to 5 ppm/500 Hz (Fig. 1 *e*) and 10 ppm/1000 Hz (Fig. 1 *g*) in the ^{15}N chemical shift/^{1}H-^{15}N dipolar coupling dimensions. Although the experimental spectra in these cases differ significantly from the ideal spectrum in Fig. 1 *c*, it is still possible to determine the helix-tilt angles with quite high accuracy from these spectra. This becomes evident from the numerical values for the τ and ρ values listed in Table 1, although the precision of the calculated helix conformations decreases as the fluctuations in resonance frequencies increase. We note that the rotational pitch becomes virtually impossible to determine as the fluctuations become large, whereas the error limits for the helix tilts remain relatively small. This observation is very encouraging, as it demonstrates that even in the case of large perturbations (10 ppm/1 kHz), the deconvolution of experimental spectra with the assumption of ideal α-helices remains stable. However, for larger proteins, as demonstrated below, the spectral complexity increases so that employing a single amino acid labeling is not sufficient; thus, we add information from differently labeled samples to increase reliability and provide unambiguous conformations of all the TM helices.

TABLE 1 Helix-tilt and rotational-pitch angles determined from simulated experimental spectra for helices 1 and 2 in the Ca^{2+} ATPase

		M1		M2	
ΔN (ppm)*	ΔNH (Hz)*	ρ (°)	τ (°)	ρ (°)	τ (°)
From crystal structure†		65.7	13.92	88.2	185.94
0	0	66 ± 5	14 ± 1	88 ± 1	186 ± 1
5	500	54 ± 20	16 ± 4	92 ± 20	185 ± 2
10	1000	70 ± 60	17 ± 10	100 ± 50	189 ± 5

*The frequencies calculated from an ideal α-helix were perturbed with a random value in the range $\pm\Delta N$ for the ^{15}N chemical shift and $\pm\Delta NH$ for the ^{1}H-^{15}N dipolar coupling.

†These values represent the helix conformation for an ideal α-helix aligned with each of helices M1 and M2 in the 1SU4 PDB structure.

With the dual aim of demonstrating the multiple residue-specific labeling approach for obtaining conformational information about large (7TM) membrane proteins, and simultaneously provide complementary structural information, bR is an ideal system. bR is a membrane protein with 7TM helices that has attracted much interest over time, not least because it is considered a model for GPCRs and is relatively easy to produce in amounts compatible with the needs for structural biology methods. Fig. 2 *a* gives a schematic representation of bR based on hydropathy plots and crystal structures (44). Here, the different labels considered in this study are highlighted in gray, and from the helix wheel plots (Fig. 2 *b*) it is evident that the seven helices have their own unique labeling pattern when considering labeling of the Gly, Met, and Val residues. This feature provides a potential route to determining helix conformation angles for all seven helices, even in the case of substantial orientational disorder (e.g., mosaic spread). The choice of labeling is a compromise between several factors:

1. Using residue-specific labeling, only residues that are not prone to biosynthetic scrambling may be used.
2. Abundant residues (like Gly and Val) provide many structural constraints, but these constraints appear as resonances in increasingly crowded spectra, whereas dilute residues (like Met) provide few, but quite precise, constraints.
3. The price of ^{15}N-labeled amino acids depends strongly on the amino acid type.
4. Amino acids with labeled side-chain nitrogens yield additional resonances that may obscure the analysis.

A series of 2D PISEMA spectra for [^{15}N]Gly-, [^{15}N]Val-, and [^{15}N]Met-bR in oriented purple membranes have been recorded, with the membrane normal parallel to the magnetic field. These spectra are shown in Fig. 3. For each of the three bR samples, two separate broad peaks located around 210

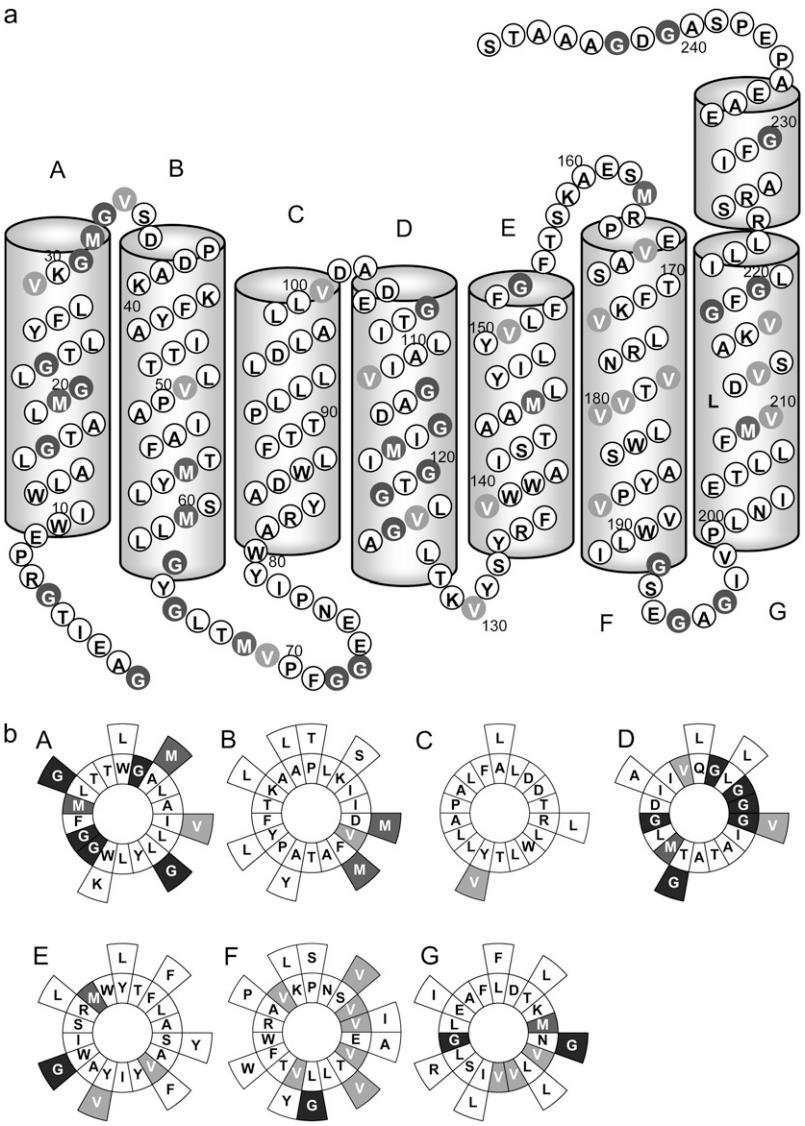

FIGURE 2 (*a*) Schematic representation of the secondary structure of bR based on the 1C3W crystal structure (44) highlighting the Gly, Val, and Met residues. (*b*) Helical wheel plots of the seven TM helices illustrating the diversity of the labeling patterns for the helices achieved by considering a combination of [^{15}N]Gly, [^{15}N]Val, and [^{15}N]Met labeling.

ppm and 60 ppm in the ^{15}N chemical shift dimension are observed, with the most intense peak, at 210 ppm, characteristic of transmembrane helices. The peak at 60 ppm is attributed to ^{15}N signals from the loop regions and from the N- and C-termini for the case of [^{15}N]Gly-bR. For comparison, Fig. 3 *a* shows the simulated PISEMA spectrum for an unoriented ''powder'' peptide sample. It is clear that the spectrum for a sample with no preferential ordering is significantly different from the experimental PISEMA spectra described here, with the most apparent difference the accumulation of intensity around 60 ppm and only weak traces of signal at higher frequencies in the ''powder'' spectrum. It is also evident from the figure that the spectral features, although not perfectly resolved, are different for the different labeling patterns.

The PISEMA spectra for the [^{15}N]Gly-, [^{15}N]Val-, and [^{15}N]Met-bR samples form a unique possibility for obtaining reliable information about the helix conformations, since these spectra provide the constraints from 35–40 helix residues as judged from the secondary-structure prediction presented in Fig. 2. Since there are no strong helix-breaking motifs (although a few prolines are present) in the 7TM helices, we will assume that each of the helices may be represented by an ideal α-helix. In support of this assumption, we note that Kim and Cross (45) reported the observation that transmembrane α-helices seem to be more ideal than is typically reported in crystal structures.

To take full advantage of the diversity in the Gly, Val, and Met ^{15}N-labeling pattern of the seven helices in bR, a simultaneous numerical analysis of the three spectra has been performed, in which the PISEMA spectra are simulated as a function of the seven pairs of helix-tilt and rotational-pitch angles, and these variables are optimized to yield the minimum root mean-square (RMS) deviation between the

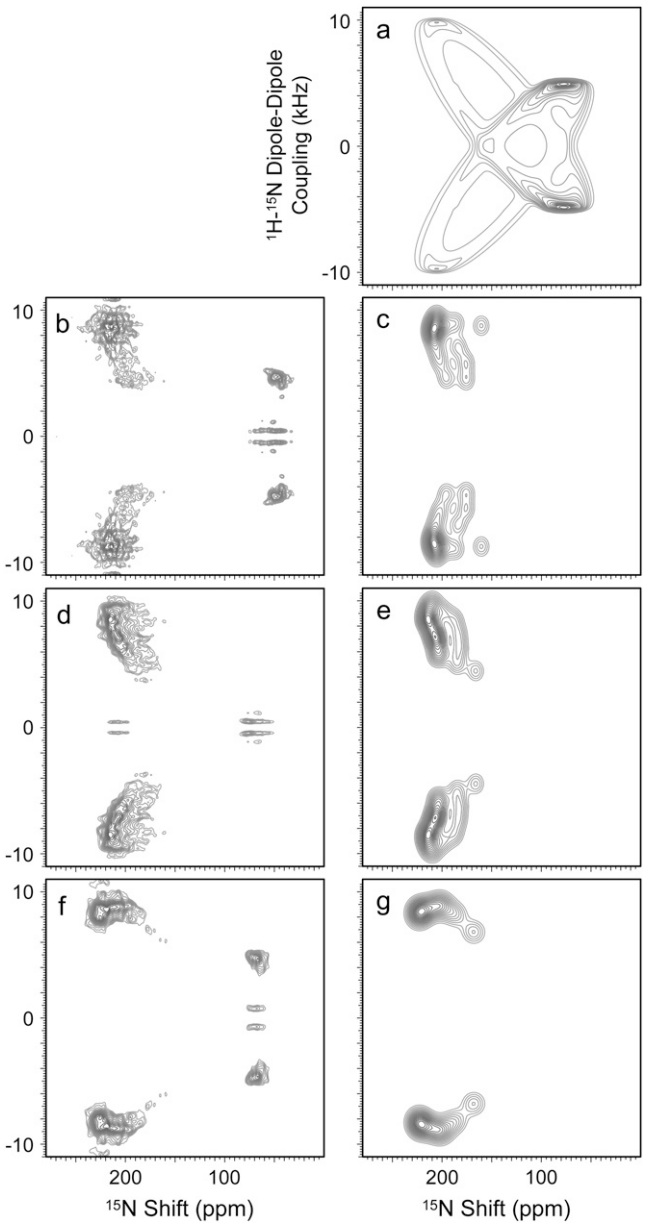

FIGURE 3 PISEMA spectra of bR. (*a*) Simulated powder spectrum employing chemical shift and dipolar coupling parameters of $\delta_{iso} = 120$ ppm, $\delta_{aniso} = 99$ ppm, $\eta_\sigma = 0.21$, and $b_{IS} = 9940$ Hz. (*b–g*) Experimental (*b*, *d*, and *f*) and simulated (*c*, *e*, and *g*) PISEMA spectra of (*b* and *c*) [^{15}N]Gly bR, (*d* and *e*) [^{15}N]Val bR, and (*f* and *g*) [^{15}N]Met bR. In all spectra, the dipolar dimension was corrected for the theoretical scaling factor $\sqrt{2/3}$. In the experimental spectra, we observe that minor peaks around zero frequency in the ^{1}H-^{15}N dipole-dipole dimension, in particular in the loop region (~60 ppm in the ^{15}N chemical shift dimension), are experimental artifacts.

simulated and experimental spectra. In addition to the helix angles, the optimizations considered variation in the resonance lineshape parameters to give the best overall match between the experimental and simulated spectra, in agreement with the estimated mosaic spread of ~5–8°, as estimated from iterative fitting of 1D and 2D spectra for the differently ^{15}N-labeled bR samples. In the PISEMA spectra, mosaic spread manifests as unique elongated lineshapes, which is taken into consideration in our numerical analysis. To avoid bias toward information from specific spectra, the RMS deviation for each of the spectra was weighted according to their signal/noise ratios as

$$RMS = \sqrt{\frac{1}{n_{Gly}+n_{Met}+n_{Val}}\left(\sum_{X=Gly,Met,Val}\frac{1}{SN_X^2}\sum_{i=1}^{n_X}\left(S_X^{exp}(i)-S_X^{sim}(i)\right)^2\right)}, \quad (1)$$

where n_X represents the number of data points in the PISEMA spectra, $S_X^{exp}(i)$ and $S_X^{sim}(i)$ the intensity in the ith experimental and simulated datapoints, respectively, in the PISEMA spectrum with labeling of amino acid X (Gly, Met, or Val), and SN_X the signal/noise ratio for this spectrum. Simulations were performed using SIMPSON (46,47) and SIMMOL (47,48) simulation software. Obviously, the numerical optimization of the 14 orientational parameters is prone to getting trapped in local minima. To reduce the possibility of such faulty interpretations, we performed a series of 1000 independent optimizations and only proceeded with data analysis for the optimizations yielding the lowest RMS deviations. To cover the 16-dimensional parameter space as thoroughly as possible, each optimization started with random input values for the seven helix tilts between 0° and 30°, whereas the random values for the rotational pitch were between 0° and 360°.

Fig. 4 *a* shows the sorted RMS deviations from these optimizations, which display a monotonically growing pattern with a single broad plateau. This may be indicative of either one well-defined global minimum or a broad continuum of solutions, whereas several plateaus in the RMS plot are typically indicative of several different solutions. It is clear from the plots of the helix-tilt angles in Fig. 4 *b*, in which the 250 optimizations with lowest RMS values have been selected, that the system here belongs to the category having a broad continuum of solutions. This does not, therefore, permit selection of the best optimizations to represent the final result because of too large a fluctuation in the tilt angles. On the other hand, the projections of the statistical distribution of the helix-tilt angles along the vertical axes in Fig. 4 reveal that there are preferential values for the helix-tilt angles for most of the helices, as observed by fits to a Gaussian distribution function. The peak positions and half-width half-heights of the resulting helix-tilt angle, and uncertainty, respectively, are given in Table 2. To demonstrate the quality of the simulations, Fig. 3, *c*, *e*, and *g*, reports typical simulated spectra for the labeled residues located in the helical regions, achieved using the helix-tilt parameters from the simulations with the lowest RMS values. We observe that the simulations for the three labeling patterns are highly different and that each matches the features in the helix part (150–220 ppm) of the corresponding experimental spectrum in a very nice manner.

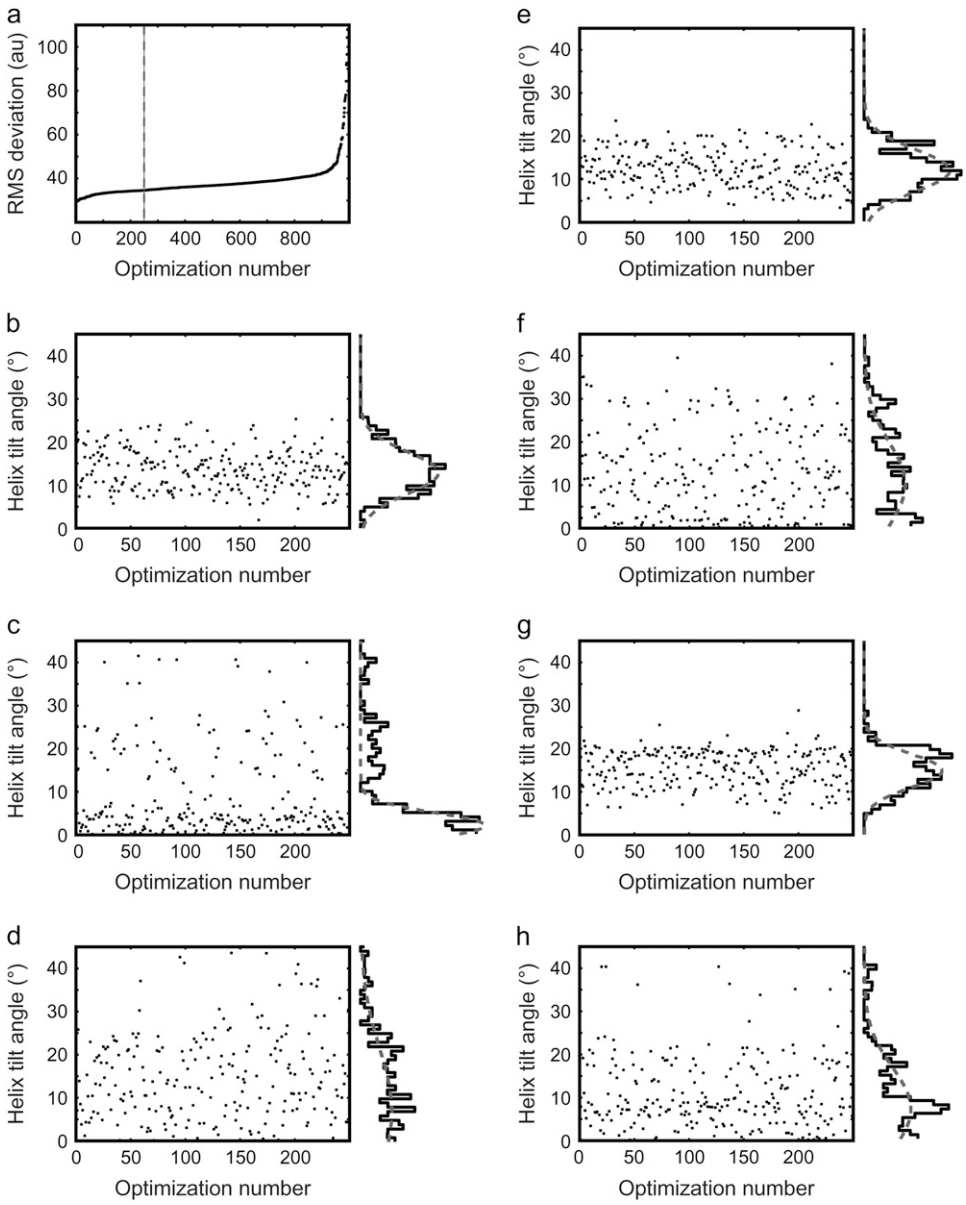

FIGURE 4 (*a*) Sorted RMS deviations between experimental and simulated PISEMA spectra including data from [^{15}N]Gly bR, [^{15}N]Val bR, and [^{15}N]Met bR. (*b–h*) Helix-tilt angles resulting from the 250 optimizations yielding the lowest RMS deviations (i.e., those to the left of the vertical dashed line in *a*), along with plots of the tilt-angle distributions (*black lines*) and best-fit Gaussian profiles (*dashed gray lines*), for helices A–G, respectively.

For evaluation of the correctness and reliability of the method described here, average, minimum, and maximum helix-tilt angles from a number of published structures of bR are given in Table 2. Good agreement between the values determined here and those previously reported by XRD determination methods is observed for most helices. In particular, the tilt angles for helices B–F agree with the XRD values within a few degrees, whereas the differences are somewhat larger for helices A and G. The origin of these deviations is not completely understood but may be ascribed to local variations in the peptide plane orientations (static or dynamical), which may be translated into uncertainties in the orientational angles of the helices by assuming ideal torsion angles. We note that the tilts of helices A, B, D, and F seem to be determined with quite high precision, whereas the precision is lower for helices C, E, and G. It can be concluded, therefore, that this method provides data of quite high precision and reliability.

It is of interest to investigate how many different labels are needed for an analysis of the kind presented here to be valuable. To address this question, analysis of the possible subsets of data using only one or two different labels was carried out. Fig. 5 shows the results of this analysis, and it is noted that the lower row corresponds to the tilt-angle distributions from Fig. 4. In Fig. 5 some of the data is missing since the labeling combination in question provided no constraints to the particular helix tilt, and hence, these labeling combinations represent highly undesirable combinations. Overall, the results from employing three labels give the best results in terms of narrow distributions, and

TABLE 2 Helix tilts for the seven transmembrane helices of bR

	Helix-tilt angles (°)				
Helix	This work	Ref. 27	Literature average	Literature minimum	Literature maximum
A	13 ± 5	18–22	24.0 ± 1.2	22.8	27.7
B	2 ± 3	1–5	4.9 ± 2.2	2.0	11.3
C	7 ± 15		9.0 ± 2.6	0.4	10.4
D	12 ± 5		8.1 ± 2.4	5.0	15.5
E	10 ± 10		12.9 ± 1.8	9.0	16.6
F	15 ± 4		14.5 ± 0.8	13.3	15.5
G	7 ± 10		16.0 ± 0.9	15.4	18.9

Literature values represent the average, minimum, and maximum tilt angles from a number of published bR structures (PDB entry codes 1AP9, 1AT9, 1C3W, 1FBB, 1IW6, 1KGB, 1M0L, 1QHJ, 1QM8, 1X0K, 1XJI, and 2AT9). The tilt angles are obtained as the tilt angle of an ideal α-helix aligned with helices from the PDB structures. The error limits on the literature average value represent the standard deviation on the angles among the 12 structures.

furthermore, combinations without the dilute Met sample generally provide rather poor results. On the other hand, using only the Met sample is not a good solution either, since helices C and F contain no Met residues, whereas helices D, E, and G each contain only one Met residue and are hence indistinguishable from the Met sample alone.

As with all rigid-atom structure determinations, this study contributes more to the structure and less to the biological understanding of bR, which is probably the most well-characterized membrane protein of all. However, it is important to emphasize the perspectives of applying this method to other, less well-characterized membrane proteins, where any structural detail provides new and important information. For this, the potential for the technique discussed here is very good. The main reason lies in sample preparation, where this method simplifies the requirement of traditional techniques like liquid-state NMR or XRD in the sample preparation. For liquid-state NMR studies, a ~40-KDa protein needs to be rapidly tumbling in solution. Although recent TROSY techniques have improved this (49,50), it still represents the major limitation of liquid-state NMR for studying large membrane proteins complexed with lipids. For XRD, the major obstacle is the difficulty in crystallizing membrane proteins and then obtaining suitable diffraction, which, for example, manifests itself in the fact that despite the enormous research and commercial interest in GPCRs, only one crystal structure for this class of proteins has been solved, namely that of rhodopsin (51), and in this case for a ground state only. Even compared to traditional approaches for solid-state NMR, either MAS or oriented-sample, this method simplifies the sample preparation, since it does not necessarily rely on high-resolution spectra and thereby most likely will turn out successfully for proteins for which a perfect alignment is not achievable.

Perhaps even more important, the method has good potential for extrapolation to functional studies. By activating a membrane-embedded protein in situ, and recording NMR spectra before and after activation, these functionally sensitive structural elements will be resolved through difference spectra. There would therefore be no need for new samples.

To apply this analysis to large membrane proteins of unknown structure, we envisage that the following procedure will be efficient. First, the putative transmembrane helices are identified in the primary structure, e.g., based on helix-propensity calculations, which permit a structural model such as the one in Fig. 1 *b* to be established. At this point, the primary sequence should be carefully analyzed for helix breaking or kinking motifs such as Gly-X-Y-Pro or just Pro residues. In the case of the presence of such motifs, each side of the helix flanking the motif should be treated as individual helices in the subsequent analysis. From the structural model, it is possible to determine the labeling patterns of the helices and choose labeled residues to maximize the difference between the helices in the NMR spectra. The rest of the data analysis may be performed as described here.

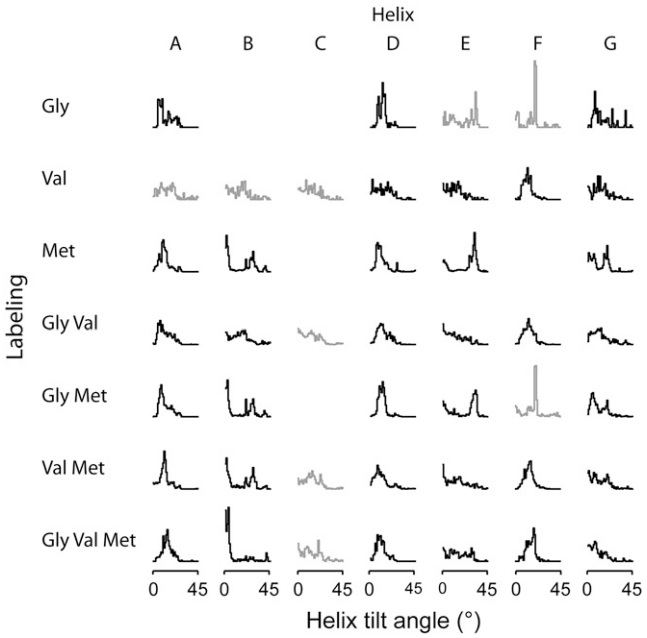

FIGURE 5 Helix-tilt distributions resulting from optimizations employing only the data listed in the leftmost column for the seven helices (A–G). Missing plots are due to the lack of data for the particular helix, and gray plots are those with only one ^{15}N label in the particular helix.

CONCLUSIONS

In conclusion, we have demonstrated that oriented-sample solid-state NMR of residue-specific labeled proteins may provide a feasible route for conformational studies of large membrane proteins, such as the 7TM receptors. This has been demonstrated by determining helix-tilt angles for bR on the basis of ^{15}N-Met, Val-, and Gly-labeled samples of bR in

native membranes. In the cases presented here, the overall alignments of the bR samples were relatively poor, with mosaic spread of 5–8°, which severely hampers a more detailed structural characterization on the one hand, but on the other hand demonstrates that a similar analysis may be performed for the class of large membrane proteins where perfect alignment of the protein containing native membranes is currently unavailable. It could be envisaged that the method will find applications for studying conformation changes upon membrane protein activation, and along with the production of better alignment protocols, the method may offer the possibility to determine full structures of large membrane proteins.

Financial support from the Danish National Research Foundation, Carlsbergfondet, the Danish Biotechnological Instrument Centre, the Danish Natural Science Research Foundation, the United Kingdom Medical Research Council, and the Bionanotechnology Interdisciplinary Research Collaboration (Oxford, U.K.) is acknowledged.

REFERENCES

1. Bernstein, F. C., T. F. Koetzle, G. J. Williams, E. F. Meyer, Jr., M. D. Brice, J. R. Rodgers, O. Kennard, T. Shimanouchi, and M. Tasumi. 1977. The Protein Data Bank: a computer-based archival file for macromolecular structures. *J. Mol. Biol.* 112:535–542.
2. Opella, S. J. 1997. NMR and membrane proteins. *Nat. Struct. Biol.* 4:845–848.
3. Watts, A., S. K. Straus, S. L. Grage, M. Kamihira, Y. H. Lam, and X. Zhao. 2004. Membrane protein structure determination using solid-state NMR. *Methods Mol. Biol.* 278:403–473.
4. Nielsen, N., A. Malmendal, and T. Vosegaard. 2004. Techniques and applications of NMR to membrane proteins. *Mol. Membr. Biol.* 21: 129–141.
5. Griffin, R. G. 1998. Dipolar recoupling in MAS spectra of biological solids. *Nat. Struct. Biol.* 5:508–512.
6. Smith, S. O., J. Hamilton, A. Salmon, and B. J. Bormann. 1994. Rotational resonance NMR determination of intra- and intermolecular distance constraints in dipalmitoylphosphatidylcholine bilayers. *Biochemistry.* 33:6327–6333.
7. Studelska, D. R., L. M. McDowell, M. Adler, R. D. O'Connor, A. K. Mehta, W. J. Guilford, J. L. Dallas, D. Arnaiz, D. R. Light, and J. Schaefer. 2003. Conformation of a bound inhibitor of blood coagulant factor Xa. *Biochemistry.* 42:7942–7949.
8. Gröbner, G., I. J. Burnett, C. Glaubitz, G. Choi, A. J. Mason, and A. Watts. 2000. Observations of light-induced structural changes of retinal within rhodopsin. *Nature.* 405:810–813.
9. Watts, A. 1999. NMR of drugs and ligands bound to membrane receptors. *Curr. Opin. Biotechnol.* 10:48–53.
10. Watts, A. 2005. Solid-state NMR in drug design and discovery for membrane-embedded targets. *Nat. Rev. Drug Discov.* 4:555–568.
11. Ketchem, R. R., K. C. Lee, S. Huo, and T. A. Cross. 1996. Macromolecular structural elucidation with solid-state NMR-derived orientational constraints. *J. Biomol. NMR.* 8:1–14.
12. Glaubitz, C., G. Grobner, and A. Watts. 2000. Structural and orientational information of the membrane embedded M13 coat protein by (13)C-MAS NMR spectroscopy. *Biochim. Biophys. Acta.* 1463: 151–161.
13. Valentine, K. G., S. F. Liu, F. M. Marassi, G. Veglia, S. J. Opella, F. X. Ding, S. H. Wang, B. Arshava, J. M. Becker, and F. Naider. 2001. Structure and topology of a peptide segment of the 6th transmembrane domain of the *Saccharomyces cerevisae* α-factor receptor in phospholipid bilayers. *Biopolymers.* 59:243–256.
14. Nishimura, K., S. Kim, L. Zhang, and T. A. Cross. 2002. The closed state of a H^+ channel helical bundle combining precise orientational and distance restraints from solid state NMR. *Biochemistry.* 41:13170–13177.
15. Castellani, F., B. van Rossum, A. Diehl, M. Schubert, K. Rehbein, and H. Oschkinat. 2002. Structure of a protein determined by solid-state magic-angle-spinning NMR spectroscopy. *Nature.* 420:98–102.
16. Zeri, A. C., M. F. Mesleh, A. A. Nevzorov, and S. J. Opella. 2003. Structure of the coat protein in fd filamentous bacteriophage particles determined by solid-state NMR spectroscopy. *Proc. Natl. Acad. Sci. USA.* 100:6458–6463.
17. Park, S. H., A. A. Mrse, A. A. Nevzorov, M. F. Mesleh, M. Oblatt-Montal, M. Montal, and S. J. Opella. 2003. Three-dimensional structure of the channel-forming trans-membrane domain of virus protein ''u'' (Vpu) from HIV-1. *J. Mol. Biol.* 333:409–424.
18. Jaroniec, C. P., C. E. MacPhee, V. S. Bajaj, M. T. McMahon, C. M. Dobson, and R. G. Griffin. 2004. High-resolution molecular structure of a peptide in an amyloid fibril determined by magic angle spinning NMR spectroscopy. *Proc. Natl. Acad. Sci. USA.* 101:711–716.
19. Heise, H., W. Hoyer, S. Becker, O. C. Andronesi, D. Riedel, and M. Baldus. 2005. Molecular-level secondary structure, polymorphism, and dynamics of full-length alpha-synuclein fibrils studied by solid-state NMR. *Proc. Natl. Acad. Sci. USA.* 102:15871–15876.
20. Lange, A., K. Giller, S. Hornig, M. F. Martin-Eauclaire, O. Pongs, S. Becker, and M. Baldus. 2006. Toxin-induced conformational changes in a potassium channel revealed by solid-state NMR. *Nature.* 440:959–962.
21. Ahmed, Z., D. G. Reid, A. Watts, and D. A. Middleton. 2000. A solid-state NMR study of the phospholamban transmembrane domain: local structure and interactions with Ca^{2+}-ATPase. *Biochim. Biophys. Acta.* 1468:187–198.
22. Harbison, G. S., S. O. Smith, J. A. Pardoen, P. P. Mulder, J. Lugtenburg, J. Herzfeld, R. Mathies, and R. G. Griffin. 1984. Solid-state 13C NMR studies of retinal in bacteriorhodopsin. *Biochemistry.* 23:2662–2667.
23. Harbison, G. S., S. O. Smith, J. A. Pardoen, C. Winkel, J. Lugtenburg, J. Herzfeld, R. Mathies, and R. G. Griffin. 1984. Dark-adapted bacteriorhodopsin contains 13-*cis*, 15-*syn*, and all-*trans*, 15-anti retinal Schiff bases. *Proc. Natl. Acad. Sci. USA.* 81:1706–1709.
24. Lakshmi, K. V., M. R. Farrar, J. Raap, J. Lugtenburg, R. G. Griffin, and J. Herzfeld. 1994. Solid state 13C and 15N NMR investigations of the N intermediate of bacteriorhodopsin. *Biochemistry.* 33:8853–8857.
25. Lewis, B. A., G. S. Harbison, J. Herzfeld, and R. G. Griffin. 1985. NMR structural analysis of a membrane protein: bacteriorhodopsin peptide backbone orientation and motion. *Biochemistry.* 24:4671–4679.
26. Hatcher, M. E., J. G. Hu, M. Belenky, P. Verdegem, J. Lugtenburg, R. G. Griffin, and J. Herzfeld. 2002. Control of the pump cycle in bacteriorhodopsin: mechanisms elucidated by solid-state NMR of the D85N mutant. *Biophys. J.* 82:1017–1029.
27. Kamihira, M., T. Vosegaard, A. J. Mason, S. K. Straus, N. C. Nielsen, and A. Watts. 2005. Structural and orientational constraints of bacteriorhodopsin in purple membranes determined by oriented-sample solid-state NMR spectroscopy. *J. Struct. Biol.* 149:7–16.
28. Saito, H., Y. Kawase, A. Kira, K. Yamamoto, M. Tanio, S. Yamaguchi, S. Tuzi, and A. Naito. 2007. Surface and dynamic structures of bacteriorhodopsin in a 2D crystal, a distorted or disrupted lattice, as revealed by site-directed solid-state C NMR. *Photochem. Photobiol.* 83:253–262.
29. Kawamura, I., N. Kihara, M. Ohmine, K. Nishimura, S. Tuzi, H. Saito, and A. Naito. 2007. Solid-state NMR studies of two backbone conformations at Tyr185 as a function of retinal configurations in the dark, light, and pressure adapted bacteriorhodopsins. *J. Am. Chem. Soc.* 129:1016–1017.
30. Park, S. H., S. Prytulla, A. A. De Angelis, J. M. Brown, H. Kiefer, and S. J. Opella. 2006. High-resolution NMR spectroscopy of a GPCR in aligned bicelles. *J. Am. Chem. Soc.* 128:7402–7403.
31. Etzkorn, M., S. Martell, O. C. Andronesi, K. Seidel, M. Engelhard, and M. Baldus. 2007. Secondary structure, dynamics, and topology of a

seven-helix receptor in native membranes, studied by solid-state NMR spectroscopy. *Angew. Chem. Int. Ed.* 46:459–462.

32. Vosegaard, T., and N. C. Nielsen. 2002. Towards high-resolution solid-state NMR on large uniformly ^{15}N- and [^{13}C,^{15}N]-labeled membrane proteins in oriented lipid bilayers. *J. Biomol. NMR.* 22:225–247.
33. Henzler Wildman, K. A., D. K. Lee, and A. Ramamoorthy. 2003. Mechanism of lipid bilayer disruption by the human antimicrobial peptide, LL-37. *Biochemistry.* 42:6545–6558.
34. Bechinger, B., and C. Sizun. 2003. Alignment and structural analysis of membrane polypeptides by ^{15}N and ^{31}P solid-state NMR spectroscopy. *Concepts Magn. Reson.* 18A:130–145.
35. Aisenbrey, C., C. Sizun, J. Koch, M. Herget, R. Abele, B. Bechinger, and R. Tampe. 2006. Structure and dynamics of membrane-associated ICP47, a viral inhibitor of the MHC I antigen-processing machinery. *J. Biol. Chem.* 281:30365–30372.
36. Aisenbrey, C., U. Harzer, G. Bauer-Manz, G. Bar, I. N. Chotimah, P. Bertani, C. Sizun, A. Kuhn, and B. Bechinger. 2006. Proton-decoupled ^{15}N and ^{31}P solid-state NMR investigations of the Pf3 coat protein in oriented phospholipid bilayers. *FEBS J.* 273:817–828.
37. Grobner, G., A. Taylor, P. T. Williamson, G. Choi, C. Glaubitz, J. A. Watts, W. J. de Grip, and A. Watts. 1997. Macroscopic orientation of natural and model membranes for structural studies. *Anal. Biochem.* 254:132–138.
38. Kamihira, M., and A. Watts. 2006. Functionally relevant coupled dynamic profile of bacteriorhodopsin and lipids in purple membranes. *Biochemistry.* 45:4304–4313.
39. Wu, C. H., A. Ramamoorthy, and S. J. Opella. 1994. High-resolution heteronuclear dipolar solid-state NMR spectroscopy. *J. Magn. Reson. A.* 109:270–272.
40. Levitt, M. H. 1991. *J. Chem. Phys.* 94:30–38.
41. Marassi, F. M., and S. J. Opella. 2000. A solid-state NMR index of helical membrane protein structure and topology. *J. Magn. Reson.* 144:150–155.
42. Wang, J., J. Denny, C. Tian, S. Kim, Y. Mo, F. Kovacs, Z. Song, K. Nishimura, Z. Gan, R. Fu, J. R. Quine, and T. A. Cross. 2000. Imaging membrane protein helical wheels. *J. Magn. Reson.* 144:162–167.
43. Toyoshima, C., M. Nakasako, H. Nomura, and H. Ogawa. 2000. Crystal structure of the calcium pump of sarcoplasmic reticulum at 2.6 Å resolution. *Nature.* 405:647–655.
44. Luecke, H., B. Schobert, H. T. Richter, J. P. Cartailler, and J. K. Lanyi. 1999. Structure of bacteriorhodopsin at 1.55 Å resolution. *J. Mol. Biol.* 291:899–911.
45. Kim, S., and T. A. Cross. 2002. Uniformity, ideality, and hydrogen bonds in transmembrane α-helices. *Biophys. J.* 83:2084–2095.
46. Bak, M., J. T. Rasmussen, and N. C. Nielsen. 2000. SIMPSON: a general simulation program for solid-state NMR spectroscopy. *J. Magn. Reson.* 147:296–330.
47. Vosegaard, T., A. Malmendal, and N. C. Nielsen. 2002. The flexibility of SIMPSON and SIMMOL for numerical simulations in solid- and liquid-state NMR spectroscopy. *Monatsh. Chem.* 133:1555–1574.
48. Bak, M., R. Schultz, T. Vosegaard, and N. C. Nielsen. 2002. Specification and visualization of anisotropic interaction tensors in polypeptides and numerical simulations in biological solid-state NMR. *J. Magn. Reson.* 154:28–45.
49. Pervushin, K., R. Riek, G. Wider, and K. Wuthrich. 1997. Attenuated T2 relaxation by mutual cancellation of dipole-dipole coupling and chemical shift anisotropy indicates an avenue to NMR structures of very large biological macromolecules in solution. *Proc. Natl. Acad. Sci. USA.* 94:12366–12371.
50. Flaux, J., E. B. Bertelsen, A. L. Horwich, and K. Wütrich. 2002. *Nature.* 418:207–211.
51. Palczewski, K., T. Kumasaka, T. Hori, C. A. Behnke, H. Motoshima, B. A. Fox, I. Le Trong, D. C. Teller, T. Okada, R. E. Stenkamp, M. Yamamoto, and M. Miyano. 2000. Crystal structure of rhodopsin: a G protein-coupled receptor. *Science.* 289:739–745.